2010

Silicon/single-walled carbon nanotube composite paper as a flexible anode material for lithium ion batteries

Shulei Chou
University of Wollongong, shulei@uow.edu.au

Yue Zhao
University of Wollongong, yue_zhao@uow.edu.au

Jiazhao Wang
University of Wollongong, jiazhao@uow.edu.au

Zhixin Chen
University of Wollongong, zchen@uow.edu.au

Hua-Kun Liu
University of Wollongong, hua@uow.edu.au

See next page for additional authors

Silicon/Single-Walled Carbon Nanotube Composite Paper as a Flexible Anode Material for Lithium Ion Batteries

Shu-Lei Chou,*,†,‡ Yue Zhao,†,§ Jia-Zhao Wang,*,†,‡ Zhi-Xin Chen,§ Hua-Kun Liu,†,‡ and Shi-Xue Dou†

Institute for Superconducting and Electronic Materials, ARC Centre of Excellence for Electromaterials Science, and Faculty of Engineering, University of Wollongong, Wollongong, NSW 2522, Australia

Received: July 9, 2010; Revised Manuscript Received: August 23, 2010

Flexible silicon/single-walled carbon nanotube (Si/SWCNT) composite paper was prepared using the pulsed laser deposition (PLD) method to deposit Si onto SWCNT paper. In the composite, Si mainly shows nanoworm-like morphology. Increasing deposition time results in an increased amount of Si microspheres. Electrochemical measurements show that the capacity of the composite paper is improved by the presence of Si. The Si/SWCNT composite with only 2.2% Si shows a capacity of 163 mA h g^{-1} at a current density of 25 mA g^{-1} up to 50 cycles, which is more than 60% improvement of the capacity of pristine CNT paper. The Si contribution in the 2.2%-Si/SWCNT sample is calculated to be higher than 3000 mA h g^{-1}.

Introduction

The rapid development of portable devices and mobile equipment requires their power supply, the Li ion rechargeable battery, to be designed with not only high energy density but also high mechanical properties, such as flexibility.[1−3] From the materials point of view, carbon nanotube (CNT) paper, which is flexible and easy to prepare, has been used as a flexible anode material for the Li ion battery.[4] However, the energy density of CNT paper is limited due to its low theoretical capacity. On the other hand, silicon is one of the most promising candidate anode materials owing to its abundance in nature, low discharge potential, and the highest known theoretical charge capacity (∼4200 mA h g^{-1}).[5,6] However, the big volume change (∼300%) during lithium insertion and extraction results in capacity fading due to pulverization and loss of electrical contact with the substrate.[7] In order to combine the advantages of both CNT paper and Si, here, we use pulsed laser deposition (PLD) to deposit silicon onto single-walled CNT (SWCNT) paper to obtain a flexible and high-performance composite paper. The as-prepared Si/SWCNT composite paper shows several advantages. First, SWCNTs can reach more than twice the energy density of graphite.[8,9] SWCNTs can also act as a free-standing, flexible, and highly conductive matrix, which can not only accommodate the large volume change but also provide good electronic contact for Si-based materials. Second, the deposited Si can improve the total specific capacity of the SWCNT paper. Finally, the amount of silicon can be controlled via changing the parameters of the PLD method.

Experimental Section

Synthesis. Single-walled CNT (SWCNT) paper was prepared using a filtration method reported previously.[4] SWCNTs (Lot No. PO323) were purchased from Carbon Nanotechnologies Inc. (CNI, USA) and used as-received without further purification. Si/SWCNT composite paper was obtained using the pulsed laser deposition (PLD) technique to deposit Si onto/into SWCNT paper. The PLD system consists of an ultraviolet (UV) excimer laser (Compex 301, $\lambda = 248$ nm from Lambda Physik) and a fixed-beam optical train, which focuses the beam onto the rotating Si target inside a vacuum chamber with a base pressure of 1×10^{-7} Torr.[10] The CNT paper was attached to a substrate stage at a distance of 50 mm from the target. The substrate temperature and the beam incident angle were fixed at ∼30 °C and 45°, respectively. The deposition conditions were laser repetition rate 5 Hz, laser pulse duration 25 ns, and energy density on the target 3.0 J/cm^2. The deposition pressure was 100 mTorr of high-purity Ar (99.999%). Different Si loadings were achieved by following the same procedure, but with different deposition time, 30 min and 2.5 h, respectively. The Si content in the composite was obtained by the weight difference in the CNT paper before and after the PLD experiment.

Instrumental Analysis. The morphology and microstructure of the as-prepared samples were characterized by X-ray diffraction (XRD; GBC MMA 017), scanning electron microscopy (SEM; JEOL FESEM-7500, 30 kV, equipped with energy-dispersive X-ray (EDX) spectroscopy), transmission electron microscopy (TEM; JEOL 2011, 200 kV), and Raman spectroscopy. Raman spectra were recorded using a JOBIN Yvon Horiba Raman spectrometer model HR800, employing a 10 mW helium/neon laser at 632.8 nm, which was filtered by a neutral density filter to reduce the laser intensity, and a charge-coupled detector (CCD).

Electrochemical Characterizations. To test the electrochemical performance, the as-prepared Si/SWCNT composite paper was cut into 0.5 cm × 0.5 cm working electrodes. The electrochemical cells (CR 2032 coin-type cell) that were prepared for testing consisted of the as-prepared Si/SWCNT composite paper as the working electrode, Li foil as the counter and reference electrode, a porous polypropylene film as separator, and 1 M $LiPF_6$ (battery grade 99.99%, Aldrich) in a 1:2 (v/v) mixture of ethylene carbonate (EC, anhydrous 99%, Sigma-Aldrich) and diethyl carbonate (DEC, anhydrous 99+%, Sigma-Aldrich) as the electrolyte. The cells were assembled in

* Corresponding authors: Tel +61-2-4298 1405; Fax +61 2 4221 5731; E-mail shulei@uow.edu.au (S.L.C.), jiazhao@uow.edu.au (J.Z.W.).
† Institute for Superconducting and Electronic Materials.
‡ ARC Centre of Excellence for Electromaterials Science.
§ Faculty of Engineering.

10.1021/jp1063403
Published on Web 08/31/2010

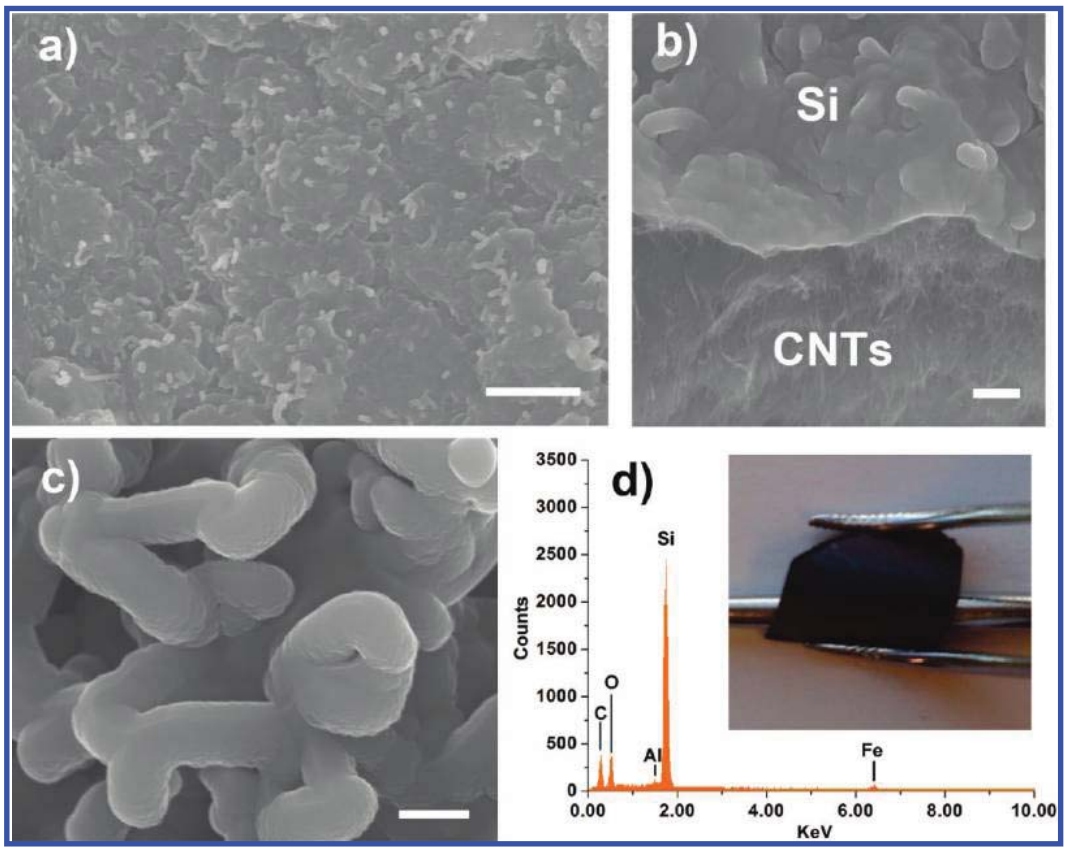

Figure 1. Typical low (a, b) and high (c) magnification SEM images of Si/SWCNT composite paper obtained from PLD with 30 min deposition time, with top (a, c) and cross-sectional (b) views. EDX spectrum (d) taken from (a). Inset of (d) is a photograph of the Si/SWCNT composite paper. The scale bar in (a), (b), and (c) is 5, 1, and 0.5 μm, respectively.

an Ar-filled glovebox. The cells were cycled at a current density of 25 mA g^{-1} between 0.01 and 2.0 V using a computer-controlled charger system manufactured by Neware battery testers. The specific capacity is based on the weight of the whole Si/SWCNT composite paper electrode. The typical electrode weight was ~1.8 mg cm^{-2}.

Results and Discussion

Structure and Morphologies. Si/single-walled CNT (Si/SWCNT) composite paper was prepared by pulsed laser deposition (PLD) of Si onto the SWCNT paper. Typical scanning electron microscope (SEM) images of the Si/SWCNT composite with deposition time of 30 min are shown in Figure 1. The low-magnification SEM image of the Si/SWCNT composite (Figure 1a) shows a large area of wormlike structures ~500 nm in diameter and 1 μm in length. The cross-sectional SEM image in Figure 1b demonstrates that the thickness of the Si deposition on the surface of the SWCNT paper is around 500 nm−1 μm. A higher magnification field emission SEM (FE-SEM) image of the Si/SWCNT composite (Figure 1c) shows several wormlike structures connected with each other. Since without using SWCNT paper PLD cannot produce this wormlike structured Si,[10] the formation of the wormlike structure is due to the presence of the SWCNTs. The morphology observed here resembles the morphology of the SWCNTs. It is possible that the Si tends to be deposited along the SWCNT surface and thus forms the wormlike structure. Figure 1d shows an energy-dispersive X-ray (EDX) spectrum taken from the area shown in Figure 1a. The EDX spectrum shows the presence of Si. The Al is coming from the SEM sample holder. The Fe is the catalyst in the CNTs. The percentage of Si in the Si/SWCNT composite paper is 2.2% for a deposition time of 30 min. The inset of Figure 1d shows a photograph of the Si/SWCNT composite paper held by tweezers, indicating the good flexibility. The surface of the paper is gray instead of black due to the deposited Si on the surface.

Typically, PLD can produce amorphous Si. In order to confirm the presence of amorphous Si, the Si/SWCNT paper composite was ground using a mortar, suspended in ethanol via ultrasonication, and loaded onto a holey carbon support film on a copper grid for TEM observations. Typical TEM images are shown in Figure 2. Figure 2a shows a broken particle, which is part of a wormlike Si structure and attached to SWCNTs. Figure 2b shows a nanoworm ~150 nm in diameter. No lattice fringes can be observed, even with high-resolution TEM (HRTEM) (not shown here), indicating the amorphous structure of the Si. The inset of Figure 2b is a selected area electron diffraction (SAED) pattern of the Si nanoworm in Figure 2b. The typical diffuse rings indicate the amorphous structure of Si. Therefore, the wormlike structure is amorphous Si.

To increase the Si content, a longer deposition time (2.5 h) was also used. Figure 3 shows typical SEM images of the Si deposited at the surface of the sample with a deposition time of 2.5 h. As shown in Figure 3a, much more and much longer rodlike Si can be observed, showing the increase in the Si content. However, there are also some microspheres on the surface. The formation of the silicon spheres is due to the further growth of the ends of the wormlike structures or to direct deposition from the Si target of PLD. Figure 3b shows a cross-sectional view of the deposited Si. The thickness of the Si layer is increased to 2−3 μm, and the wormlike structure is more condensed than for the film prepared in 30 min. The Si content is around 11% in the Si/SWCNT composite with a deposition time of 2.5 h.

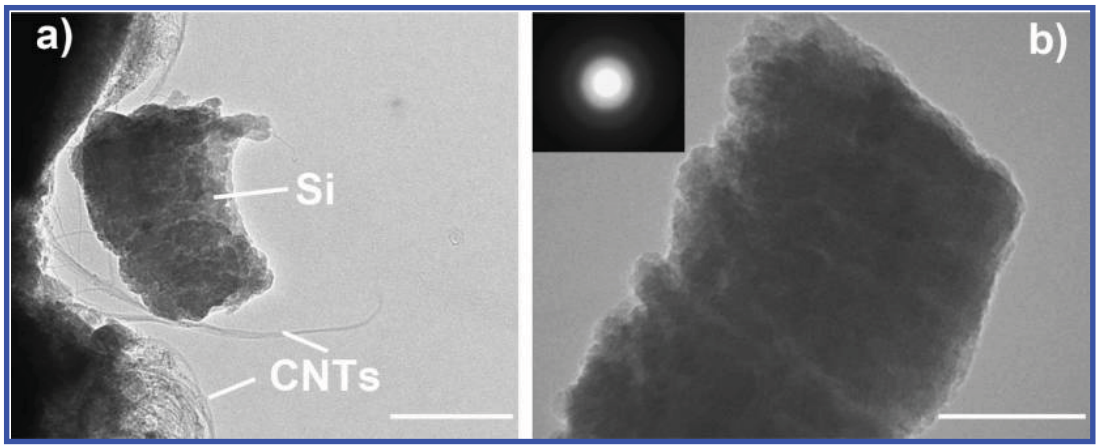

Figure 2. Typical TEM images (a) and (b) of Si/SWCNT composite. The inset of (b) is the corresponding SAED pattern. The scale bars in (a) and (b) are 100 nm.

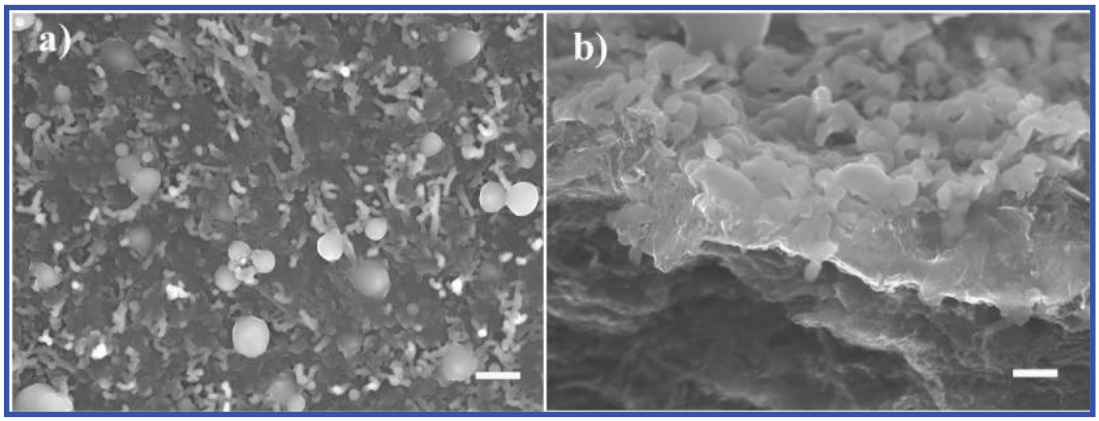

Figure 3. SEM images showing top (a) and cross-sectional (b) views of Si/SWCNT composite paper prepared by PLD with a 2.5 h deposition time. The scale bar in (a) and (b) is 2 and 1 μm, respectively.

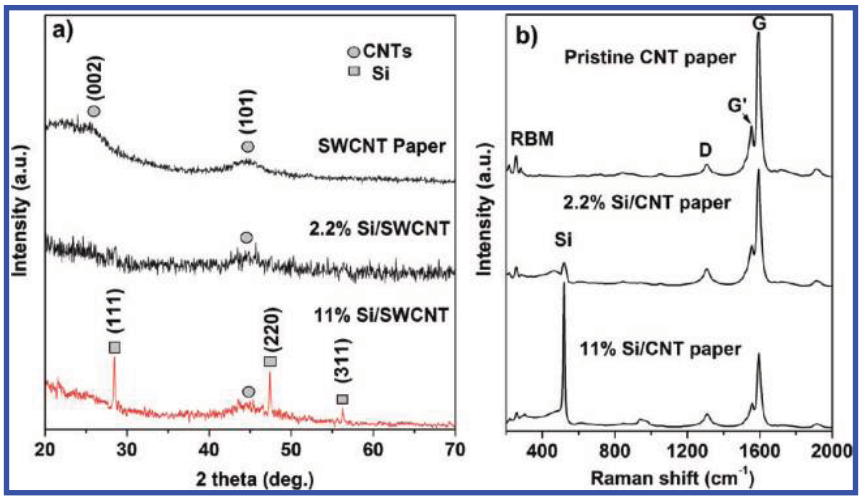

Figure 4. (a) XRD patterns and (b) Raman spectra of pristine CNT paper and Si/CNT composite paper with 2.2% and 11% of Si contents.

X-ray diffraction (XRD) patterns and Raman spectra for the Si/SWCNT composite paper are shown in Figure 4. All the diffraction peaks in the XRD patterns of the 11%-Si/SWCNT composite paper (Figure 4a) can be indexed to cubic Si phase with space group $Fd\bar{3}m$ (JCPDS no. 77-2108), except for the broad peak at around 45°, which is due to the SWCNT paper. No peaks of any other phases were detected. There is no diffraction peaks for the 2.2%-Si/SWCNT composite paper except the broad peak at around 45° from SWCNT, showing the amorphous structure of Si in 2.2%-Si/SWCNT sample. Since PLD produces amorphous wormlike Si in a short deposition time, the crystallized Si observed here is probably due to the spherical Si which came from the Si target. Raman spectra (Figure 4b) confirmed the presence of both crystallized Si in 11%-Si/SWCNT composite paper with a band located at 520 cm^{-1} and the SWCNTs with D, G′, and G bands around 1310, 1556, and 1596 cm^{-1}, respectively. In the low Si content of 2.2%-Si/SWCNT sample, a small broad Si peak can be observed, indicating the presence of amorphous Si. The radial breathing mode (RBM) of SWCNTs located below 400 cm^{-1} was also observed in the Si/SWCNT composite paper,[11] showing that the structure of the SWCNTs remains.

Electrochemical Characterization. Figure 5 shows the charge−discharge curves and their corresponding differential

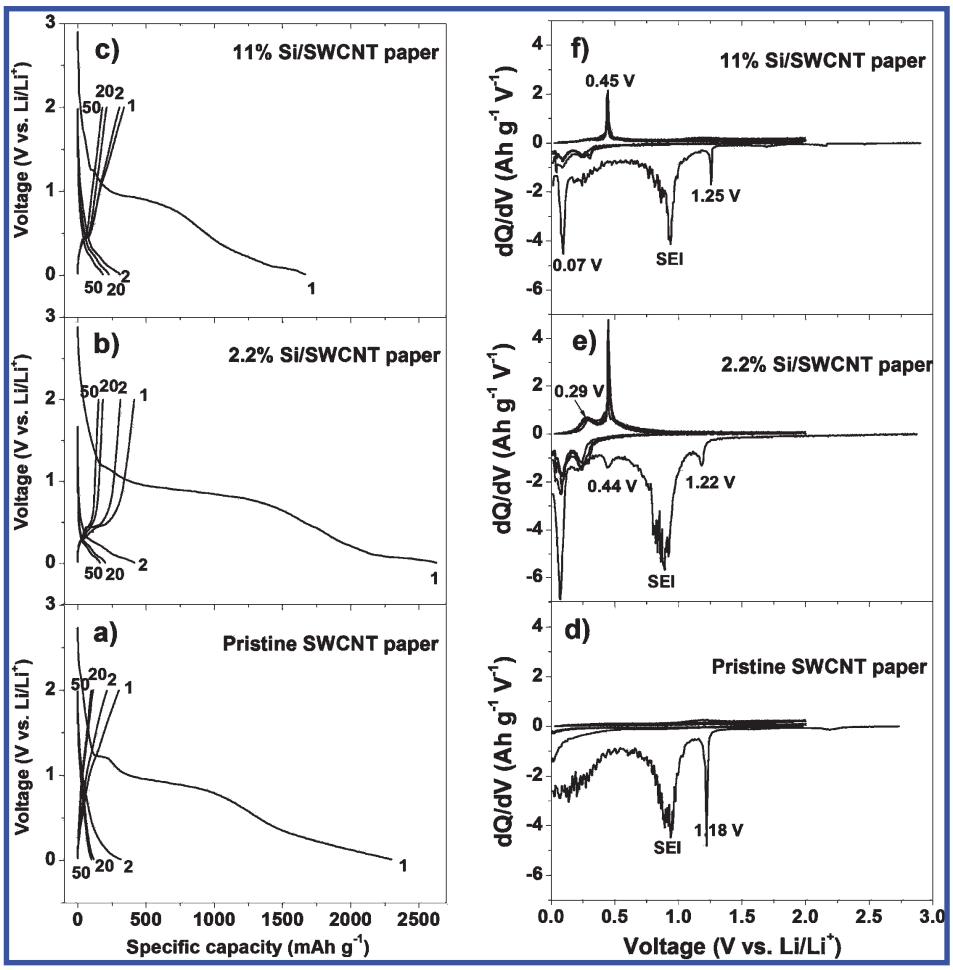

Figure 5. Charge−discharge curves (a−c) and their differential profiles (d−f) of pristine SWCNT paper (a, c) and Si/SWCNT composite paper with 2.2% (b, e) and 11% (c, f) Si tested in coin cells at 25 °C.

profiles for the pristine SWCNT paper and Si/SWCNT composite paper electrodes in the coin cells at a current density of 25 mA g^{-1} between 0.01 and 2.0 V vs Li/Li^+. The pristine SWCNT paper electrode (Figure 5a) shows a large initial discharge capacity of ∼2300 mA h g^{-1}, but the first charge capacity is low, only 300 mA h g^{-1} with a low Coulombic efficiency of around 13%. After 20 cycles, the pristine SWCNT paper shows a relatively stable discharge capacity of around 110 mA h g^{-1} and an average Coulombic efficiency of ∼96%. The results observed here are similar to those in a previous report on SWCNTs.[4] From the differential plots of the charge−discharge curves (Figure 5d), three peaks can be observed during the first discharge process. A sharp peak at 1.2 V vs Li/Li^+ can be seen for the pristine SWCNT paper. This peak is due to the reduction of surface species containing oxygen on SWCNTs.[12] The broad peak at 0.8−0.9 V vs Li/Li^+ is attributed to the formation of the solid electrolyte interphase (SEI) layer.[13] Another broad peak at lower potential (below 0.5 V vs Li/Li^+) mainly arises from the Li ion intercalation into the graphitic-type layers. No obvious peak can be observed in the following cycles, indicating the large irreversible reaction.

Figure 5b,c shows typical charge and discharge curves of the Si/SWCNT composite paper. The 2.2%-Si/SWCNT composite paper electrode shows an initial discharge capacity of 2628 mA h g^{-1} with a Coulombic efficiency of 16%, which is slightly higher than that of the pristine SWCNT paper, while the 11%-Si/SWCNT composite paper only shows an initial capacity of 1668 mA h g^{-1}. The second discharge capacity of the 2.2%-Si/SWCNT composite is 412 mA h g^{-1}, which is much better than that of the pristine SWCNT paper, while the 11%-Si/SWCNT composite only shows a capacity of 310 mA h g^{-1}. Here, we need to point out that the electrode with the most Si loading rate shows the lowest initial capacity. The reason is that the irreversible capacity of single wall CNT is the major contribution to the initial capacity of Si/SWCNT composite. On the one hand, the 11% loading rate of Si reduced the contact between SWCNT and electrolyte and then reduced the initial capacity. On the other hand, the crystallized big ball-like structure cannot react with lithium totally due to the low conductivity of this free-standing binder free film electrode. So the initial capacity of highest Si loading rate is the lowest one instead of the highest one. Therefore, the 11%-Si/SWCNT shows lower initial capacity and the second discharge capacity than that of 2.2%-Si/SWCNT electrode.

The dQ/dV profiles of the Si/SWCNT composite paper electrode are shown in Figure 5e,f. The peak at around 1.2 V vs Li/Li^+ is reduced significantly, indicating the modification of the surface of the SWCNT paper due to the Si coating. The peak at 0.8−0.9 V related to SEI layer formation is still broad and big for 2.2%-Si/SWCNT sample, but much smaller for the 11%-Si/SWCNT composite paper, indicating that the large Si coated onto the SWCNT paper had an effect on the SEI layer. A sharp peak at 0.07 V was also observed during the first discharge for both samples, which was due to the phase transition of amorphous Li_xSi to crystalline $Li_{15}Si_4$.[14,15] Upon the second discharge, two peaks were observed at 0.24 and 0.08 V for the both Si/SWCNT composite paper electrodes, in contrast to the first discharge. The peaks at 0.23 and 0.08 V

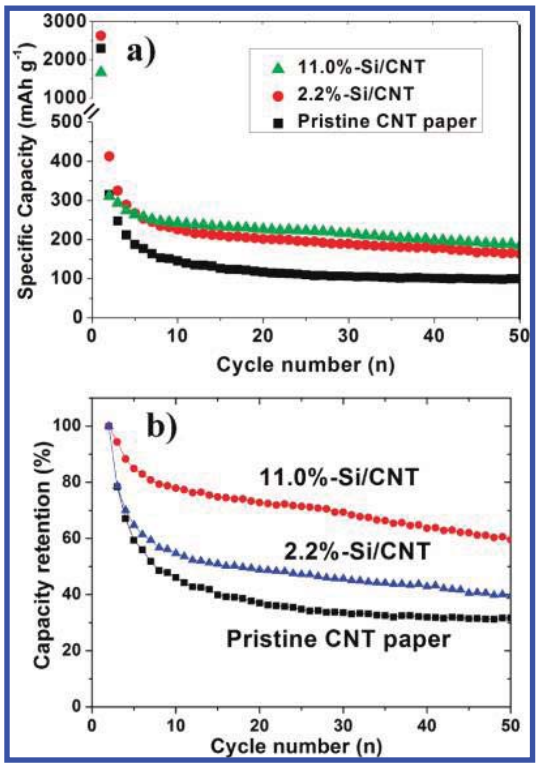

Figure 6. Cycle life (a) and capacity retention (b) of pristine SWCNT paper and Si/SWCNT composite paper electrode with silicon contents of 2.2% and 11.0% at a current density of 25 mA g^{-1}. The cycles are all between 0.01 and 2.0 V vs Li/Li^+ at 25 °C.

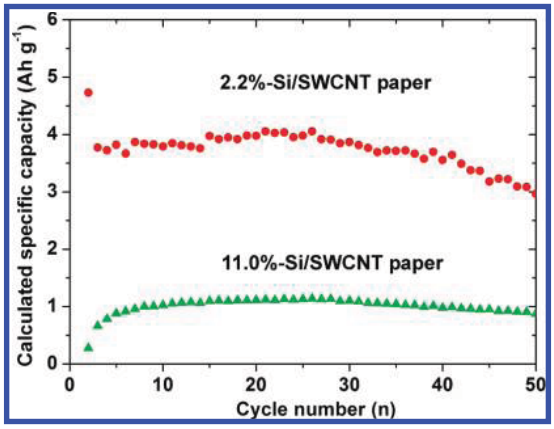

Figure 7. Calculated discharge capacity of Si for Si/SWCNT composite electrode with silicon contents of 2.2% (circles) and 11.0% (triangles). The cycles are all between 0.01 and 2.0 V vs Li/Li^+ at 25 °C.

may be due to the phase transitions between amorphous Li_xSi. Here, the intensities of the peaks of the Si/SWCNT composite paper remained almost the same, showing the great enhancement of the cycling stability. For the charge, a sharp peak was observed at 0.45 V for both composites, which is usually observed in silicon during first charge, indicating the presence of Si in the Si/SWCNT composite. An additional small peak with a peak potential at 0.29 V was observed for 2.2%-Si/SWCNT composite, which is usually seen in amorphous silicon thin films as well as in bulk amorphous silicon from the second charge onward,[16,17] indicating the presence of amorphous Si for the 2.2%-Si/SWCNT composite. For 11%-Si/SWCNT composite, the peak at around 0.3 V is relatively small, indicating that the Si is mostly crystallized. The presence of both crystalline Si and amorphous Si was thus confirmed for 11%-Si/SWCNT composite, which is in good agreement with the XRD, Raman, and TEM results.

The cycling stabilities of the pristine SWCNT paper electrode and the Si/SWCNT composite paper electrode are shown in Figure 6a. The discharge capacity of the Si/SWCNT composite paper with 11.0% and 2.2% Si at the 50th cycle are 189 and 163 mA h g^{-1}, respectively. The capacity retention curves are shown in Figure 6b. It can be seen that the capacity retention is in the order of the Si content. The Si/SWCNT composite paper with 11.0% Si shows the best capacity retention. More than 60% reversible capacity is retained after 50 cycles for the 11.0%-Si/SWCNT sample, while only 40% and 30% reversible capacity can be retained for the 2.2%-Si/SWCNT sample and the pristine SWCNT paper, respectively. The Si coating not only improves the specific capacity but also enhances the capacity retention. The enhanced capacity retention may be due to the modification of the SWCNT surface via the deposition of Si.

The calculated pure Si contribution to the specific capacity (Q_{Cal}) is obtained from eq 1

$$Q_{Cal} = \frac{Q_M - Q_{CNT}C_{CNT}}{C_{Si}} \quad (1)$$

where Q_M is the specific capacity of the Si/SWCNT composite paper, Q_{CNT} is the specific capacity of corresponding cycle of the pristine SWCNT paper, and C_{CNT} and C_{Si} are the percentages of SWCNTs and Si in the composite, respectively. The calculated contribution of pure Si from the Si/SWCNT composite is shown in Figure 7. It can be seen that Si in the 2.2%-Si/SWCNT sample shows a relatively stable calculated capacity of ~3700 mA h g^{-1} for more than 40 cycles, which almost reaches the theoretical capacity (4200 mA h g^{-1}). After 40 cycles, the calculated capacity starts to decrease quickly to 3000 mA h g^{-1} at the 50th cycle. The high capacity indicates the high utilization of Si during the lithium alloying and dealloying. The possible reason is that the Si nanoworms are electrically connected to the SWCNTs, so that all the Si nanoworms will contribute to the capacity and the electron transport will be enhanced. On the contrary, the 11.0%-Si/SWCNT composite paper electrode only shows a calculated capacity of around 1000 mA h g^{-1}. The possible reason is the presence of microsize crystalline Si spheres, which can only totally react with lithium at a very low current density.[15]

Previous reports showed that Si-based nanostructured materials, such as crystalline Si nanowires,[18] crystalline−amorphous core−shell Si nanowires,[19] mesoporous Si@carbon nanowires,[20] Si nanotubes,[21] and Si/graphene composite,[22] have excellent electrochemical performance. Moreover, a Si/CNT composite was reported to have a capacity of 950 mA h g^{-1} after 20 cycles.[23] Here, the specific capacity is much lower than the previous reported value[18−24] as well as commercial graphite (300 mA h g^{-1}). The reason is that the as-prepared Si/SWCNT paper electrode is a free-standing and totally flexible electrode. Considering the total weight of the electrode from the previous report, the present work is very promising. Here, the limitation will be the loading rate of Si. However, to maintain the good mechanical properties of SWCNT paper, the Si loading rate cannot be very high. Furthermore, the formation of the microsize Si spheres at high Si content (11%) also lowers the utilization of Si in the composite according to our calculation. There is still room to improve the performance in the future either via carefully synthesizing the SWCNT paper so that it is thinner, but still has good mechanical properties, or by optimizing the ratio of SWCNTs to Si.

Conclusions

Flexible silicon/single-walled carbon nanotube (Si/SWCNT) composite paper was prepared using the pulsed laser deposition (PLD) method to deposit Si onto SWCNT paper. In the composite, Si shows nanoworm-like morphology. An increased deposition time results in an increased amount of Si microspheres. Electrochemical measurements showed that the capacity of the composite paper was improved due to the presence of the nanoworm-like Si. The Si contribution in the 2.2%-Si/SWCNT sample is calculated to be higher than 3000 mA h g^{-1} up to 50 cycles. The high utilization of Si is due to the fact that Si nanoworms are electrically connected with the SWCNTs, so that all the Si nanoworms will contribute to the capacity and the electron transport will be enhanced.

Acknowledgment. Financial support provided by the Australian Research Council (ARC) through a Discovery project (DP0987805) and ARC Centre of Excellence funding (CE0561616) is gratefully acknowledged. The authors also thank Dr. T. Silver for critical reading of the manuscript.

References and Notes

(1) Service, R. F. *Science* **2006**, *313*, 902.

(2) Pushparaj, V. L.; Shaijumon, M. M.; Kumar, A.; Murugesan, S.; Ci, L.; Vajtai, R.; Linhartd, R. J.; Nalamasu, O.; Ajayan, P. M. *Proc. Natl. Acad. Sci. U.S.A.* **2007**, *104*, 13574.

(3) Hu, L. B.; Choi, J. W.; Yang, Y.; Jeong, S.; La Mantia, F.; Cui, L. F.; Cui, Y. *Proc. Natl. Acad. Sci. U.S.A.* **2009**, *106*, 21490.

(4) Chew, S. Y.; Ng, S. H.; Wang, J. Z.; Novak, P.; Krumeich, F.; Chou, S. L.; Chen, J.; Liu, H. K. *Carbon* **2009**, *47*, 2976.

(5) Weydanz, W. J.; Wohlfahrt-Mehrens, M.; Huggins, R. A. In *9th International Meeting on Lithium Batteries*; Edinburgh: Scotland, 1998; p 237.

(6) Obrovac, M. N.; Christensen, L. *Electrochem. Solid State Lett.* **2004**, *7*, A93.

(7) Wolfenstine, J. *J. Power Sources* **1999**, *79*, 111.

(8) Iwai, Y.; Hirose, M.; Kano, R.; Kawasaki, S.; Hattori, Y.; Takahashi, K. *J. Phys. Chem. Solids* **2008**, *69*, 1199.

(9) Gao, B.; Kleinhammes, A.; Tang, X. P.; Bow, C.; Fleming, L.; Wu, Y.; Zhou, O. *Chem. Phys. Lett.* **1999**, *307*, 153.

(10) Park, M. S.; Wang, G. X.; Liu, H. K.; Dou, S. X. *Electrochim. Acta* **2006**, *51*, 5246.

(11) Rao, A. M.; Richter, E.; Bandow, S.; Chase, B.; Eklund, P. C.; Williams, K. A.; Fang, S.; Subbaswamy, K. R.; Menon, M.; Thess, A.; Smalley, R. E.; Dresselhaus, G.; Dresselhaus, M. S. *Science* **1997**, *275*, 187.

(12) Lu, W.; Chung, D. D. L. *Carbon* **2001**, *39*, 493.

(13) Fong, F.; Sacken, K.; Dahn, J. R. *J. Electrochem. Soc.* **1990**, *137*, 2009.

(14) Obrovac, M. N.; Christensen, L. *Electrochem. Solid State Lett.* **2004**, *7*, A93.

(15) Li, J.; Dahn, J. R. *J. Electrochem. Soc.* **2007**, *154*, A156.

(16) Hatchard, T. D.; Dahn, J. R. *J. Electrochem. Soc.* **2004**, *151*, A838.

(17) Datta, M. K.; Kumta, P. N. *J. Power Sources* **2009**, *194*, 1043.

(18) Chan, C. K.; Peng, H. L.; Liu, G.; McIlwrath, K.; Zhang, X. F.; Huggins, R. A.; Cui, Y. *Nature Nanotechnol.* **2008**, *3*, 31.

(19) Cui, L. F.; Ruffo, R.; Chan, C. K.; Peng, H. L.; Cui, Y. *Nano Lett.* **2009**, *9*, 491.

(20) Kim, H.; Cho, J. *Nano Lett.* **2008**, *8*, 3688.

(21) Song, T.; Xia, J. L.; Lee, J. H.; Lee, D. H.; Kwon, M. S.; Choi, J. M.; Wu, J.; Doo, S. K.; Chang, H.; Park, W.; Zang, D. S.; Kim, H.; Huang, Y. G.; Hwang, K. C.; Rogers, J. A.; Paik, U. *Nano Lett.* **2010**, *10*, 1710.

(22) Chou, S. L.; Wang, J. Z.; Choucair, M.; Liu, H. K.; Stride, J. A.; Dou, S. X. *Electrochem. Commun.* **2010**, *12*, 303.

(23) Shu, J.; Li, H.; Yang, R. Z.; Shi, Y.; Huang, X. J. *Electrochem. Commun.* **2006**, *8*, 51.

(24) Wang, W.; Kumta, P. N. *ACS Nano* **2010**, *4*, 2233.

JP1063403